PROCEEDINGS OF SCIENCE

DESY 10-019
SFB/CPP-10-21

arXiv:1002.0925v1 [hep-lat] 4 Feb 2010

Status and prospects for the calculation of hadron structure from lattice QCD

Dru B. Renner*
NIC, DESY, Platanenallee 6, D-15738 Zeuthen, Germany
E-mail: dru.renner@desy.de

Lattice QCD calculations of hadron structure are a valuable complement to many experimental programs as well as an indispensable tool to understand the dynamics of QCD. I present a focused review of a few representative topics chosen to illustrate both the challenges and advances of our community: the momentum fraction, axial charge and charge radius of the nucleon. I will discuss the current status of these calculations and speculate on the prospects for accurate calculations of hadron structure from lattice QCD.

The XXVII International Symposium on Lattice Field Theory
July 26-31, 2009
Peking University, Beijing, China

*Speaker.

© Copyright owned by the author(s) under the terms of the Creative Commons Attribution-NonCommercial-ShareAlike Licence.

1. Introduction

Our most stringent constraints on the structure of any hadron follow from the underlying symmetries of QCD. Translational invariance dictates that the momentum of a hadron is the sum of the momenta of all its constituents, giving rise to a powerful sum rule for the nucleon. Rotational invariance demands that the spins of hadrons have the values $n/2$ for an integer n, hence the nucleon spin is precisely $1/2$ and not 0.5 with some experimental error. Similarly, we know that the electric charge of the nucleon is exactly 1 and the net strangeness is 0. These statements are so commonplace that they may even appear trivial, but each of these exact results serves as an entry to different aspects of the dynamics of QCD.

The momentum of the nucleon is built up from that of the quarks and gluons. While translational symmetry constrains the entire contribution, the individual contributions of each quark flavor and the gluon depend on the details of QCD. Similarly, the spin of the nucleon arises from the quark spin, quark orbital motion and the gluon angular momentum, each of which are individually unconstrained by symmetries but must sum to $1/2$. The charge of the nucleon arises from the quark charges that yield a total charge of 1, but the distribution of this charge in the spatial degrees of freedom probes the nonperturbative structure of the nucleon. Finally, the strange quarks in the nucleon occur in precisely matched pairs of quarks and anti-quarks. Despite the net absence of strangeness, the consequences of this hidden flavor are felt in many observables. In the following, I will elaborate on a few of these points and discuss what we currently know from lattice calculations, phenomenology and experimental measurements. Along the way, I'll offer my opinion regarding where our calculations may have to go to provide accurate results for hadron structure.

The past several years have seen extensive reviews of the calculations presented each year at the annual Lattice conference. You can find the few most recent reviews in [1, 2, 3], and a very recent and exhaustive collection of results can be found in [4]. Rather than duplicating these efforts, I will instead present some of the key examples mentioned above.[1] This will unfortunately prohibit me from discussing all the hadron structure efforts presented at Lattice 2009, but I hope these proceedings will still provide a useful overview, nonetheless.

2. Nucleon Momentum

The momentum of a nucleon with energy E and mass m is precisely constrained by Lorentz symmetry as $p^2 = E^2 - m^2$. This is such a common statement in particle physics that it seems nearly trivial to even mention it. However, here we want to question how this momentum arises from the underlying QCD degrees of freedom. In other words, what is the distribution of this momentum among the nucleon's constituents? This question concerns the details of the dynamics of QCD and presents a challenge to lattice calculations of nucleon structure.

2.1 Parton Distribution Functions

The proper field theoretic response to the question above requires constructing the momentum distributions of the nucleon's constituents, the parton distribution functions (PDFs). I'll pro-

[1] At the lattice conference I discussed strangeness in the nucleon. A recent review [5] covers much of this, so I will not include these results in this review.

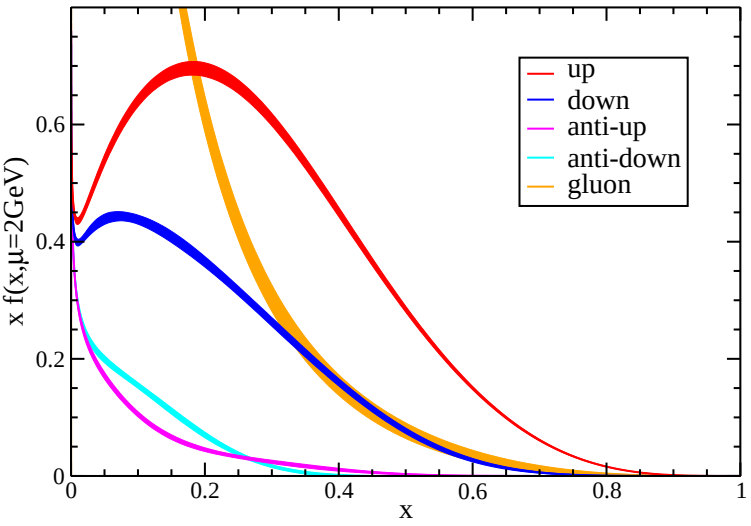

Figure 1: Momentum distribution of quarks and gluons in the nucleon at $\mu = 2$ GeV. For each parton $xf(x,\mu)$ is plotted where $f(x,\mu)$ is the corresponding PDF. At large x, the up and down quarks are the largest components of the nucleon momentum. At low x, the gluon dominates and the anti-quark distributions grow. The curves were generated using the LHAPDF library [6] and the MSTW2008 NNLO [7] dataset at a renormalization scale of $\mu = 2$ GeV.

vide a proper definition of the PDFs shortly, but for the moment we want to focus on a more intuitive understanding of the quark and gluon distributions, $q(x)$ and $g(x)$. In the parton model $q(x)$ or $g(x)$ would be the probability to find a quark, of some flavor, or a gluon with momentum $p_{\text{parton}} = x p_{\text{nucleon}}$. This interpretation is retained in QCD, however, $q(x,\mu)$ and $g(x,\mu)$ now carry a renormalization scale μ that loosely gives the energy resolution at which the distribution is probed. While this muddies the picture a bit, the PDFs, nonetheless, are well-defined universal properties of the nucleon that are probed in many different experiments.

2.1.1 Phenomenological Results for PDFs

There is now a well-established industry dedicated to extracting the PDFs from global analyses. The analyses differ in many details, including the order of the perturbative expansion used, the treatment of the quark masses and the handling of the statistical and systematic errors from the many experimental inputs. These variations have an impact on the precision ultimately obtained, however, these details do not impact the discussion at hand. Hence, as merely one example among several, I show the PDFs from the MSTW collaboration in Fig. 1.

Field theory effects ultimately handicap any simple interpretation of the PDFs, however, we can still see that the PDFs at a low scale, $\mu = 2$ GeV in Fig. 1, retain features that one might expect for the nucleon. The up and down quark distributions are the largest component for high momentum ($x \lesssim 1$). These distributions in fact have peaks at reasonable values of x, as one might expect for a

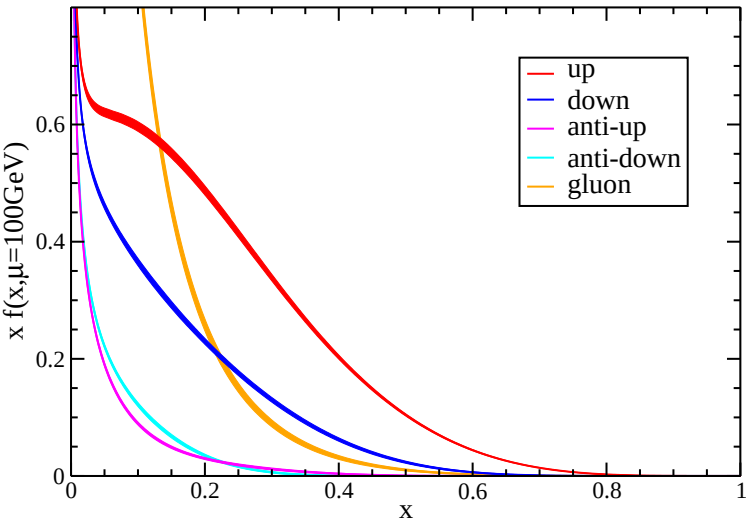

Figure 2: Momentum distribution of quarks and gluons in the nucleon at $\mu = 100$ GeV. The details are the same as in Fig. 1 but now $\mu = 100$ GeV. At high scales, the PDFs for the quarks and gluons mix and the simple non-relativistic nucleon structure, still visible at $\mu = 2$ GeV, is suppressed at $\mu = 100$ GeV.

hadron dominantly composed of two up quarks and one down quark. However, the most prominent feature in the plot for low x is clearly the gluon distribution. This is a clear indication of QCD physics at work. This has a counterpart in the simple observation that the quark masses directly contribute only about 1% of the nucleon's mass. Beyond the dynamics of QCD, the presence of the anti-quarks is a striking field theory effect. This statement may seem mundane, but we must remember the role played by the anti-quarks in nucleon structure to appreciate why we go through all the difficulty to calculate hadronic matrix elements from fully dynamical lattice QCD rather than being content with models or quenched calculations.

As mentioned, field theory complicates the interpretation of the PDFs. To illustrate this, I show the same distributions again in Fig. 2 but now evolved to a scale of $\mu = 100$ GeV. Any hint of nucleon physics is now well hidden and all the constituents of the nucleon appear to play nearly equally important roles. We will return to this issue again when discussing the evolution of the momentum fraction.

2.1.2 Operator Definition of PDFs

The parton distribution functions can be defined as nucleon matrix elements of quark and gluon fields separated by light-like distances. As an example, we record here the operator definition of the unpolarized quark distribution $q(x,\mu^2)$ [8],

$$q(x,\mu^2) = \frac{1}{2}\int\frac{d\lambda}{2\pi}\, e^{ixp\cdot\lambda n}\langle p,s|\,\overline{q}(-\lambda/2\,n)\,\not{n}\,W_n(-\lambda/2\,n,\lambda/2\,n)\,q(\lambda/2\,n)\,|p,s\rangle|_{\mu^2}\,. \qquad (2.1)$$

For each flavor there are two other twist-two quark distributions, the helicity and transversity distributions, denoted as $\Delta q(x,\mu^2)$ and $\delta q(x,\mu^2)$ respectively. The factor $W_n(-\lambda/2\,n,\lambda/2\,n)$ is the Wilson line extending along the arbitrary light-cone direction n from $\lambda/2\,n$ to $-\lambda/2\,n$,

$$W_n(-\lambda/2\,n,\lambda/2\,n) = \mathscr{P}exp\left(ig\int_{-\lambda/2}^{\lambda/2} d\alpha\, A(\alpha n)\cdot n\right).$$

The scale, μ, and scheme dependence of $q(x,\mu^2)$ comes from the renormalization of the operator in Eq. 2.1.

The expression in Eq. 2.1 highlights the difficulty of lattice calculations of PDFs. Lattice QCD calculations are performed in Euclidean space, however, the PDFs involve quark and gluon fields separated along the light-cone. These inherently Minkowski-space observables are difficult to construct explicitly in Euclidean space. But, as we will see in the next section, the moments in x of these distributions can be calculated directly in Euclidean space.

2.2 Moments of Parton Distributions

As just discussed, the PDFs as a function of x are essentially Minkowski-space objects. But the moments in x are related to local operators that can be calculated in Euclidean space on the lattice.

2.2.1 Mellin Transform: from x to n

The moments in x are defined as follows,

$$\langle x^n\rangle_{q,\mu^2} = \int_{-1}^{1} dx x^n q(x,\mu^2) = \int_0^1 dx x^n \left\{q(x,\mu^2) - (-1)^n \overline{q}(x,\mu^2)\right\}.$$

The sign in the above equation is determined by the identification of $q(x)$ for negative x with the anti-quark distribution as $\overline{q}(x,\mu^2) = -q(-x,\mu^2)$.[2] These moments can be related to forward matrix elements of twist-two operators. First we present the complete result but then sketch the argument in the following.

$$\langle p,s|\,\overline{q}(0)\,\gamma^{\{\mu_1}\,iD^{\mu_2}\cdots iD^{\mu_n\}}q(0)\,|p,s\rangle|_{\mu^2} = 2\langle x^n\rangle_{q,\mu^2}\,p^{\{\mu_1}\ldots p^{\mu_n\}} \tag{2.2}$$

The brackets in $T^{\{\mu_1\cdots\mu_n\}}$ denote symmetrization of the indices of the tensor T and subtraction of the traces. The precise meaning of this operation will be clarified shortly.

The derivation of Eq. 2.2 is almost elementary, but it is so essential to the method underlying the lattice calculations that we sketch the arguments using the unpolarized PDFs as an example. The first step is to introduce light-cone coordinates and gauge. This is a useful first step in understanding several aspects of the PDFs. In defining the light-cone coordinates, you introduce two light-cone directions $n_\pm^\mu = (1,0,0,\pm1)/\sqrt{2}$. The two new light-cone coordinates are given by $v\cdot n_\pm = v^\mp$ for a four-vector v. (Similarly, $\not{n}_\pm = \gamma\cdot n_\pm = \gamma^\mp$.) Light-cone gauge is the choice of $A(x)\cdot n = 0$,

[2] This is a frequent source of confusion when comparing to phenomenological determinations of the PDFs. Also note that the sign is different for the transversity distribution but the same for the helicity distribution: $\delta\overline{q}(x,\mu^2) = \delta q(-x,\mu^2)$ and $\Delta\overline{q}(x,\mu^2) = -\Delta q(-x,\mu^2)$.

which sets the Wilson line $W_n(-\lambda/2\,n, \lambda/2\,n)$ to 1. Then choosing $n = n_-$ in Eq. 2.1, imposing the light-cone gauge for n_- and relabeling λ as y^- gives

$$q(x,\mu^2) = \frac{1}{2}\int \frac{dy^-}{2\pi}\, e^{ixp^+y^-} \langle p,s|\, \overline{q}(-y^-/2)\, \gamma^+\, q(y^-/2)\, |p,s\rangle|_{\mu^2}\,. \tag{2.3}$$

The next step in relating the moments to local operators is to use the known limited support of $q(x)$ to the region $-1 \le x \le 1$ to expand the integration range used to define the moments,

$$\langle x^n\rangle_{q,\mu^2} = \int_{-1}^{1} dx x^n q(x,\mu^2) = \int_{-\infty}^{\infty} dx x^n q(x,\mu^2)\,.$$

The remaining steps are relatively elementary. The key sequence follows from combining the above with Eq. 2.3,

$$\int_{-\infty}^{\infty} dx x^n e^{ixp^+y^-} = (ip^+)^{-n}\int_{-\infty}^{\infty} dx\, (\partial^+)^n e^{ixp^+y^-} =$$

$$= (-1)^n (ip^+)^{-n}\int_{-\infty}^{\infty} dx e^{ixp^+y^-}(\partial^+)^n = (p^+)^{-n}\delta(p^+y^-)(i\partial^+)^n$$

where $\partial^+ = \partial/\partial y^-$. The above manipulations must be understood as acting under the $\int dy^-$ in Eq. 2.3. The final result is

$$\langle x^n\rangle_{q,\mu^2} = 2^{-1}(p^+)^{-(n+1)}\langle p,s|\, \overline{q}(0)\, \gamma^+\, (i\partial^+)^n q(0)\, |p,s\rangle|_{\mu^2}\,.$$

By inspection, this expression can be seen as the light-cone coordinate, light-cone gauge form of the following

$$\langle p,s|\, \overline{q}(0)\, \not{n}\, (in\cdot D)^n q(0)\, |p,s\rangle|_{\mu^2} = 2\langle x^n\rangle_{q,\mu^2}(n\cdot p)^{n+1}\,.$$

This expression relates $\langle x^n\rangle_{q,\mu^2}$ to diagonal matrix elements of local operators. The more familiar form follows from writing the above as

$$n_{\mu_1}n_{\mu_2}\ldots n_{\mu_n}\langle p,s|\, \overline{q}(0)\, \gamma^{\mu_1}\, iD^{\mu_2}\cdots iD^{\mu_n} q(0)\, |p,s\rangle|_{\mu^2} = 2\langle x^n\rangle_{q,\mu^2}\, n_{\mu_1}\ldots n_{\mu_n} p^{\mu_1}\ldots p^{\mu_n}\,.$$

This form makes it clear precisely what the symmetrization and trace removal in Eq. 2.2 means.

2.2.2 Phenomenology of $\langle \mathbf{x}\rangle_{\mathbf{u-d}}$

The global analysis illustrated in Figs. 1 and 2 can also be used to examine the moments of the PDFs. This time taking as an example the results from the CTEQ collaboration, I plot the results for $\langle x\rangle_q$ and $\langle x\rangle_g$ in Fig. 3. These results follow from numerically integrating curves similar to those in Figs. 1 and 2. Furthermore, the state-of-the-art results for the particular quantity of interest to us, $\langle x\rangle_{u-d}$, are collected in Tab. 1. The phenomenological analyses often present results in terms of the so-called valence distribution $q_v(x) = q(x) - \overline{q}(x)$ and the anti-quark distribution $\overline{q}(x)$, but Tab. 1 gives the correct combination that is comparable to lattice results.

What is particularly interesting about the momentum fraction $\langle x\rangle$ is that it obeys a sum rule,

$$1 = \sum_q \langle x\rangle_{q,\mu^2} + \langle x\rangle_{g,\mu^2} \tag{2.4}$$

[3]The error given in [14] is asymmetric, but here we take only the upper error to compare to the lattice results that are all higher than the phenomenological values.

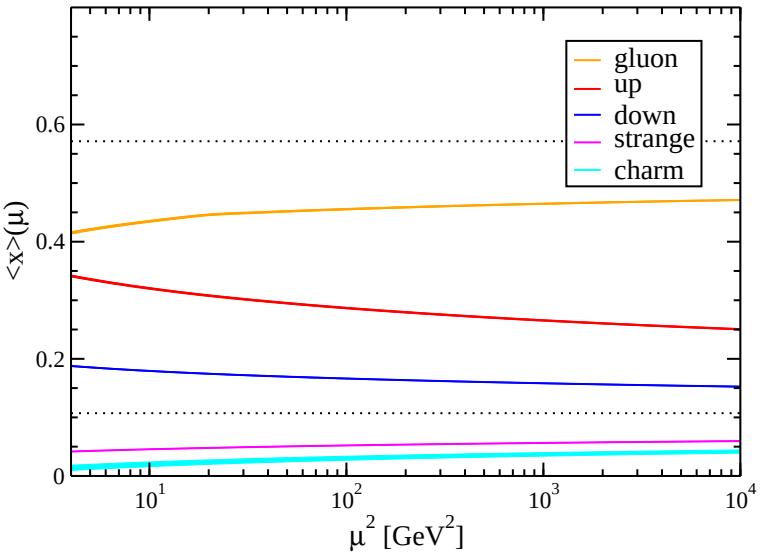

Figure 3: Running of the momentum fraction of the quarks and gluons in the nucleon. As μ increases, the gluon momentum fraction $\langle x\rangle_g$ increases towards the asymptotic value of $4/7$ and $\langle x\rangle_q$, for each of the quark flavors, approaches the common value of $3/28$. (These values hold for the 4 flavor theory.) Despite the unique limiting values for x, the non-perturbative input at low μ clearly dictates the values of the momentum fraction for each parton over many orders of magnitude. The results come from the LHAPDF library [6] using the CTEQ6.6C [9] dataset.

where $\sum_q$ is the sum over all relevant flavors. This sum rule imposes constraints on the scale evolution of $\langle x\rangle_{\mu^2}$ such that $\langle x\rangle_{\mu^2}$ asymptotically approaches a perturbatively calculable limit for large μ.

$$\lim_{\mu\to\infty}\langle x\rangle_{q,\mu^2} = \frac{3}{16+3N_{\rm F}}$$

$$\lim_{\mu\to\infty}\langle x\rangle_{g,\mu^2} = \frac{16}{16+3N_{\rm F}}$$

For $N_{\rm F}=4$, we have $\lim\langle x\rangle_q = 3/28 \approx 10\%$ and $\lim\langle x\rangle_g = 4/7 \approx 60\%$. However, we can clearly see in Fig. 3 that the asymptotic results for $\langle x\rangle$ bear little resemblance to the results at any reasonable value of μ. In fact, the hierarchy shown in Fig. 3 is quite clear. The gluons carry about 40% of the nucleon momentum, the up and down quarks carry about 35% and 20%, and the strange takes most of the remaining 5%. It is precisely this pattern that we eventually hope to understand from lattice calculations.

2.3 Lattice Calculation of $\langle x\rangle_{u-d}$

The lowest non-trivial moments of the unpolarized quark PDFs are $\langle x\rangle_q$.[4] These are the quark contributions that enter the momentum sum rule in Eq. 2.4. Here I use the particular combination

[4]The lowest moments $\langle 1\rangle_q$ are known in terms of the quark valence structure of the nucleon.

	$[x]_{u_v-d_v}$	$\langle x\rangle_{u-d}$
ABMK	0.1790 ± 0.0023	0.1646 ± 0.0027
BBG	0.1747 ± 0.0039	0.1603 ± 0.0041
JR	0.1640 ± 0.0060	0.1496 ± 0.0062
MSTW	0.1645 ± 0.0046[3]	0.1501 ± 0.0048
AMP06	0.1820 ± 0.0056	0.1676 ± 0.0058
BBG	0.1754 ± 0.0041	0.1610 ± 0.0043

Table 1: Phenomenological values for $\langle x\rangle_{u-d}$ at $\mu = 2$ GeV. For each calculation we give the moment of the non-singlet valence distribution, denoted by $[x]_{u_v-d_v}$. (The square brackets denote simply the integral over the region $0 \leq x \leq 1$ as opposed to the region $-1 \leq x \leq 1$ used in the angular brackets.) These values were collected in [10]. The original references are [10] (ABMK), [11, 12] (BBG), [13] (JR), [14] (MSTW), [15] (AMP06) and [11, 12] (BBG N^{3}LO). This is combined with the result $[x]_{\overline{u}-\overline{d}} = -0.0072 \pm 0.0007$ from [10] to produce a result for $\langle x\rangle_{u-d}$, which can be compared to lattice calculations.

$\langle x\rangle_{u-d}$ as a benchmark observable to evaluate the lattice calculation of moments of PDFs.

$$\langle p,s|\overline{q}\gamma^{\{\mu}\, iD^{\nu\}}\tau^3 q|p,s\rangle\Big|_{\mu^2} = 2\langle x\rangle_{u-d,\mu^2} p^{\{\mu}\, p^{\nu\}}$$

Here $q = (u,d)$ is the doublet of the light quarks. The flavor combination $u-d$ eliminates disconnected diagrams, which would otherwise require a substantial computational investment. Additionally, this combination also eliminates any mixing with gluonic operators, thus greatly simplifying the renormalization of this quantity. [5] Without the mixing, this observable then only requires a multiplicative renormalization. Finally, you can calculate the bare matrix elements using nucleons with $\vec{p} = 0$. Hence, $\langle x\rangle_{u-d}$ is basically the most accurate scale-dependent observable in nucleon structure that we calculate on the lattice.

Figure 4 illustrates all the dynamical lattice QCD results for $\langle x\rangle_{u-d}$ for pion masses less than 700 MeV. The values for $\langle x\rangle_{u-d}$, m_π and a come from a variety of already published sources and numerous private communications. (The references are provided in the caption to Fig. 4.) The most striking feature that you observe in Fig. 4 is that, despite the community's efforts to calculate with many actions, several lattice spacings and volumes and a broad range of pion masses now approaching 250 MeV, the calculations still overestimate the experimental measurement by at least 30% and maybe as much as a factor of 2. The spread amongst the groups obviously suggests some systematic variations, and I will examine two possible explanations shortly, but it is important to note that the individual calculations are visibly much more consistent with themselves than with the other calculations. Additionally, notice that some groups are beginning to perform calculations "at the physical point," as illustrated by the QCDSF calculation in Fig. 4. This phrase quite often means simply $m_\pi < 200$ MeV. Nonetheless, the next generation of lattice calculations will likely shed some much needed light on the chiral behavior. However, the discrepancy amongst the groups at pion masses where we should be able to reliably calculate today is an issue that needs to be

[5] Strictly speaking, the disconnected diagrams and the mixing with gluons only vanish for lattice actions with an exact flavor symmetry.

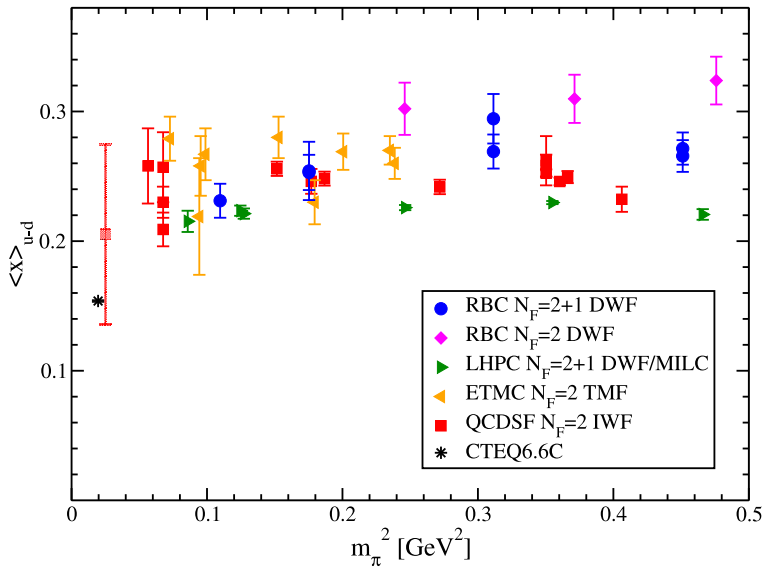

Figure 4: World's dynamical lattice QCD results for $\langle x \rangle_{u-d}$. The lattice calculations all overestimate the phenomenologically determined value. They also show a fair amount of scatter amongst themselves. The possible role of finite size and renormalization effects are discussed in the text. The lattice results are from [16, 17, 18] (RBC $N_F = 2+1$), [19, 20] (RBC $N_F = 2$), [21] (LHPC), [22, 23] (ETMC) and [24] (QCDSF). The experimental result is generated using the LHAPDF library [6] and the CTEQ6.6C dataset [9].

addressed. Without resolving these discrepancies, it will be hard to confidently establish physical results even with calculations approaching the physical pion mass.

Before discussing finite size and renormalization effects, I want to make a quick comment on the lattice spacing dependence of $\langle x \rangle_{u-d}$. This is currently poorly studied. Of the five calculations shown in Fig. 4, only QCDSF has calculated beyond a single lattice spacing. However, even in that case, the range in a that is used to establish scaling is not large. Their results are an encouraging hint that lattice artifacts are not a substantial part of the discrepancy in Fig. 4, but there is nothing universal about such effects and all the groups must make a stronger effort to calculate at multiple lattice spacings.

A persistent concern in nucleon structure calculations is the role of finite size effects. In fact, the results at Lattice 2009 have added much to this issue even if they haven't resolved it. In Fig. 5, I examine several finite size studies by various collaborations. Excluding the lightest calculations at $m_\pi = 260$ MeV, one observes no statistically significant finite size effects for any of the remaining calculations. These results are consistent with the common rule-of-thumb that $m_\pi L \approx 4$ is sufficient. [6] However, the recent results of QCDSF at $m_\pi = 260$ MeV potentially stand in contrast to the finite size dependence observed at higher pion masses. This calculation suggests that $m_\pi L = 4$ is at best just barely sufficient to capture the large volume limit of $\langle x \rangle_{u-d}$. It is

[6] My use of $m_\pi L$ to gauge finite size effects is, of course, not strictly correct. I am loosely assuming a discussion in or near the chiral limit in which $1/m_\pi$ will be the dominant length scale.

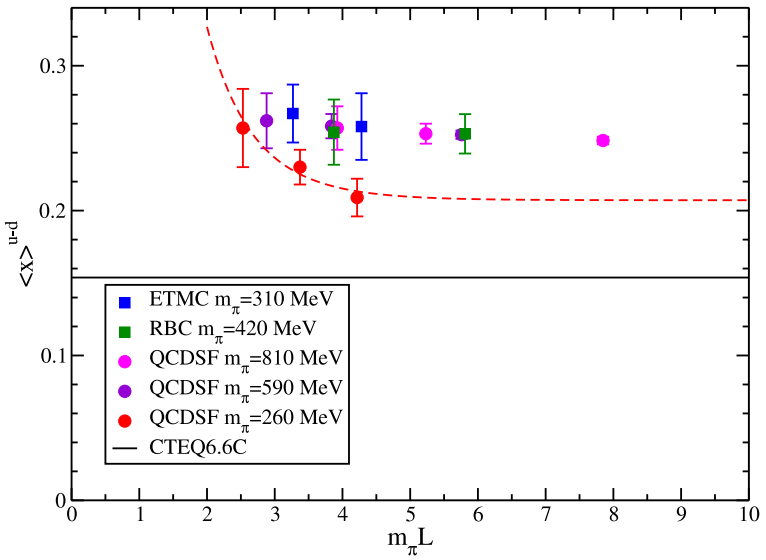

Figure 5: Finite size studies for $\langle x \rangle_{u-d}$. The dependence of $\langle x \rangle_{u-d}$ on $m_\pi L$ is shown for several calculations. Notice the essentially flat behavior for $m_\pi L > 4$ for all but the lightest pion mass. The QCDSF calculation at the lightest pion mass may suggest the emergence of a more substantial finite size effect as m_π is decreased. The curve is a very simple scaling to the $m_\pi = 260$ MeV results and is meant solely to guide the eye. The results are from the same references given in Fig. 4.

possible that this observation would vanish with higher statistics. In fact, the three calculations at $m_\pi = 260$ MeV do essentially agree statistically, but the trend in the results is suggestive, especially in comparison to all the other results at larger m_π. Of course, it is also possible that $\langle x \rangle_{u-d}$ would drop even further with still larger L.

In a review of this nature it is difficult to perform a detailed infinite volume limit of all the results presented at the conference. However, we can illustrate the impact of finite size effects by simply making the crude restriction to $m_\pi L > 4$. This is illustrated in Fig. 6. The picture is certainly clearer and one may even be left with the impression of some downward curvature for some of the lattice calculations, but we must guard against wishful thinking. Excluding the QCDSF results, each of the groups is statistically consistent with a linear dependence on m_π^2 with $\chi^2/\text{dof} < 0.75$. The one exception is QCDSF. A linear fit gives $\chi^2/\text{dof} = 2.1$. This is not overwhelming evidence of non-linearity and all the apparent curvature comes solely from the lightest point at $m_\pi = 260$ MeV. This point is 2.8σ less than the second lightest QCDSF point. Increased statistics in these calculations and confirmation of this new finite size behavior by other groups will be necessary to understand what is happening at $m_\pi = 260$ MeV.

Given the results in Figs. 5 and 6, there is no concrete conclusion that we can draw yet regarding finite size effects, but I hope that Fig. 5 will stand as a warning that the finite size effects can, and likely do, change substantially as we decrease the pion mass and that collaborations pushing towards the physical pion mass must keep these effects in mind. At this point one may argue that we should investigate the finite size effects as indicated from chiral perturbation theory. It is my

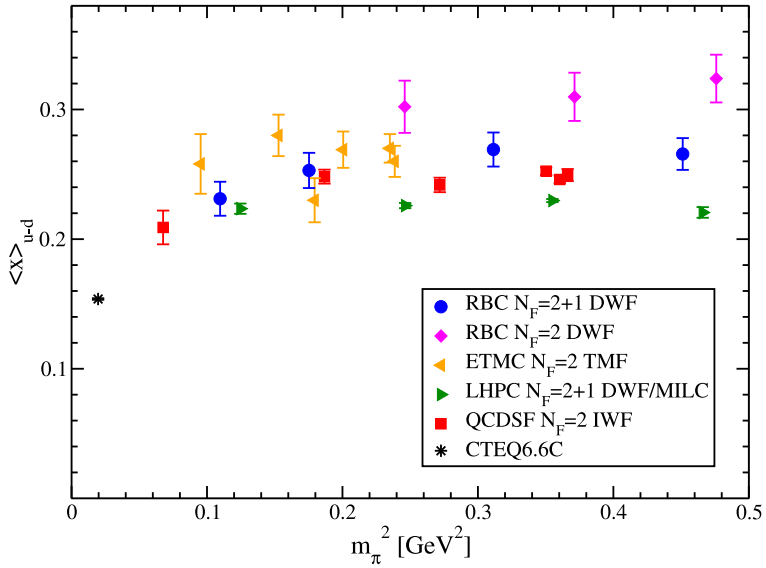

Figure 6: Large volume results for $\langle x \rangle_{u-d}$. The results are from the same references given in Fig. 4, but only those calculations with $m_\pi L > 4$ are shown. The results from each calculation are consistent with a smooth, nearly flat m_π dependence. However there is a systematic variation between the calculations.

personal opinion that, given an absence of any real evidence for curvature in $\langle x \rangle_{u-d}$ and given that such non-analytic behavior is the hallmark of chiral perturbation theory, it is theoretically questionable to force a fit to chiral perturbation theory. While this is my opinion, it was clear at the lattice conference that many presenters also simply chose to not show chiral fits. Of course, calculations at still lighter pion masses may show the expected chiral behavior and systematic errors at the current pion masses may obscure this behavior, but we should keep in mind that in the end calculations down to the physical point may be necessary to convincingly establish results for $\langle x \rangle_{u-d}$.

One obvious feature of Fig. 6 is that the results from each collaboration have a flat behavior but there are clear shifts between the groups. One natural concern in this respect is the renormalization of the operator used to determine $\langle x \rangle_{u-d}$. This is multiplicative and, importantly, quark mass independent. However it does depend on the lattice action and hence will vary between the different calculations. By taking the ratio of $\langle x \rangle_{u-d}$ to the value $\langle x \rangle^{\rm ref}_{u-d}$ at some canonical reference mass, which I arbitrarily choose to be $m_\pi = 500$ MeV, we can eliminate the renormalization factor consistently for each calculation. The result of this is shown in Fig. 7, and we find that the various calculations appear to collapse onto a universal curve. As with the finite size effects, we can not make a specific conclusion, but this result is suggestive of potential problems in the renormalization of $\langle x \rangle_{u-d}$. There are other possible explanations of the systematic shifts between the groups, such as the lattice spacing effects mentioned earlier or systematics due to plateaus that are too short in the bare matrix element calculations [19, 25]. Independent of the ultimate explanation for these problems, I hope that the difference between Fig. 6 and Fig. 7 encourages us to examine the systematics of our calculations.

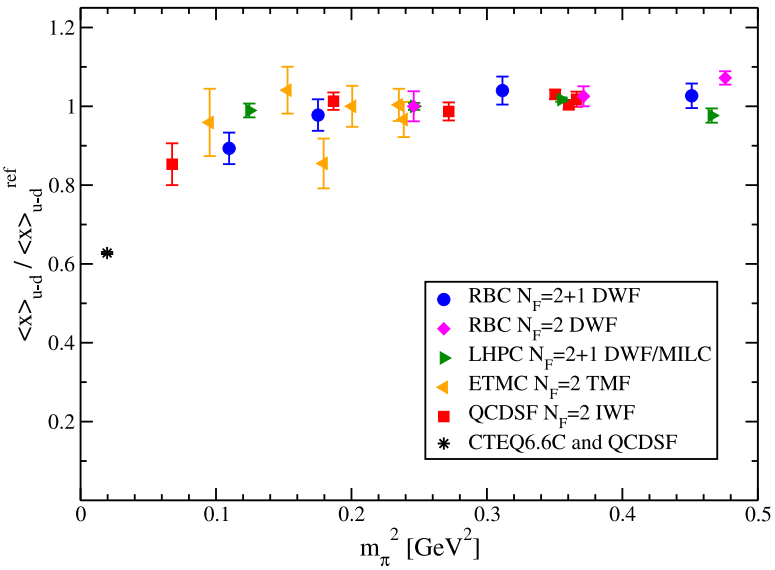

Figure 7: Renormalization free ratio: $\langle x\rangle_{u-d}/\langle x\rangle^{\text{ref}}_{u-d}$. The calculations with $m_\pi L > 4$ from Fig. 6 are used to form the ratio $\langle x\rangle_{u-d}/\langle x\rangle^{\text{ref}}_{u-d}$, where the reference scale is chosen as $m_\pi^{\text{ref}} = 500$ MeV. This ratio eliminates the renormalization factors from each calculation. The calculations are now all consistent with each other. This demonstrates that a systematic error, possibly in the renormalization, could possibly account for the discrepancy among the collaborations.

3. Nucleon Spin

As discussed in the introduction, the nucleon spin is exactly $1/2$ due to rotational symmetry, and similar to the momentum fraction, it obeys a sum rule [26],

$$\frac{1}{2} = \frac{1}{2}\sum_q \langle 1\rangle_{\Delta q,\mu^2} + \sum_q L_{q,\mu^2} + J_{g,\mu^2}\,, \tag{3.1}$$

which relates the nucleon spin to the contributions from quark helicity $\langle 1\rangle_q$ and orbital angular momentum L_q and a net contribution from the gluons J_g. The asymptotic evolution of the total quark contribution $J_q = \frac{1}{2}\sum_q \langle 1\rangle_{\Delta q} + \sum_q L_q$ and the total gluon contribution J_g is given by

$$\lim_{\mu\to\infty} J_{q,\mu^2} = \frac{1}{2}\frac{3N_{\text{F}}}{16+3N_{\text{F}}}$$

$$\lim_{\mu\to\infty} J_{g,\mu^2} = \frac{16}{16+3N_{\text{F}}}\,.$$

For $N_{\text{F}} = 4$, we find $\lim J_q = 2/7 \approx 0.60\cdot 1/2$ and $\lim J_g = 3/14 \approx 0.40\cdot 1/2$. Again we find the gluons playing a substantial role, now in the nucleon spin and earlier in the nucleon momentum. This is a particularly surprising conclusion in light of the naive quark model result $\sum_q \langle 1\rangle_{\Delta q} = 1$ and $J_g = 0$. However, similar to the asymptotic results for the momentum fraction, we should be suspicious that non-perturbative QCD dynamics can alter the picture at low scales.

Unfortunately, much less is known experimentally regarding the decomposition of the nucleon spin. The one quantity that is known well is the axial coupling, $g_A = \langle 1 \rangle_{\Delta u} - \langle 1 \rangle_{\Delta d}$, that is measured accurately in neutron beta decay. A recent review [27] gives $g_A = 1.2750(9)$ and the most recent PDG [28] world average is $g_A = 1.2694(28)$. The remaining quark contributions are essentially the only other known pieces. The experimental result from HERMES in 2007 [29] gives $\langle 1 \rangle_{\Delta u} = 0.842(12)$, $\langle 1 \rangle_{\Delta d} = -0.427(12)$ and $\langle 1 \rangle_{\Delta s} = -0.085(17)$. QCD sum rules [30] or model estimates [31] indicate that $J_g \approx 0.25$ at low scales. Taking the experimental results for $\langle 1 \rangle_{\Delta q}$ and this estimate for J_g, we can estimate that 50% of the nucleon spin is given by the gluons with the remaining divided into 33% from quark spin and 18% from quark orbital motion. This picture is much less certain than the momentum sum rule, but again, it provides a challenge to the lattice QCD effort.

3.1 Lattice Calculation of g_A

The nucleon axial charge can be defined by

$$\langle p, s | \overline{q} \gamma_\mu \gamma_5 \tau_3 q | p, s \rangle = 2 g_A s_\mu$$

or $g_A = \langle 1 \rangle_{\Delta u - \Delta d}$. The moments $\langle 1 \rangle_{\Delta q}$ are the lowest moments of the polarized PDFs. For the unpolarized distributions, the moments $\langle 1 \rangle_q$ are fixed by the valence structure of the nucleon, but this is not the case for the polarized distribution. This difference actually makes the moments $\langle 1 \rangle_{\Delta q}$ even simpler than the momentum fractions, $\langle x \rangle_q$, discussed in the previous section. In fact, using a lattice action with chiral symmetry would eliminate the need to renormalize the lattice operator used to determine $\langle 1 \rangle_{\Delta q}$ altogether.[7] However, many lattice actions in use today do require this renormalization, but it is not scale dependent and is in many ways simpler than the renormalization required for $\langle x \rangle_q$. Additionally, since the power of x in $\langle 1 \rangle_{\Delta q}$ is one lower than in $\langle x \rangle_q$, the lattice operator does not contain a derivative and is a simple quark bilinear. Consequently, the bare matrix elements can be calculated more accurately for $\langle 1 \rangle_{\Delta q}$ than for $\langle x \rangle_q$. As in the case of $\langle x \rangle_{u-d}$, we focus on the $u-d$ combination again to eliminate the computationally demanding disconnected diagrams. Furthermore, this combination gives the axial coupling $g_A = \langle 1 \rangle_{\Delta u - \Delta d}$ that is very accurately measured in neutron beta decay.

In Fig. 8, I collect all the full QCD lattice results for g_A, again with $m_\pi < 700$ MeV. Similar to $\langle x \rangle_{u-d}$, g_A serves as a benchmark observable for lattice calculations of nucleon structure. As in Fig. 4 for $\langle x \rangle_{u-d}$, we find that the lattice results show a degree of scatter and all consistently underestimate the experimental measurement. However, the discrepancy, between 10% and 20%, is more mild and the scatter in the lattice results is less severe. In fact, as I try to argue next, it appears that this scatter may be almost entirely accounted for by finite size effects, at least to the current level of statistical precision.

In Fig. 9, I examine several finite size studies that are available for g_A. The results for the heaviest values of the pion mass show a strong finite size effect. This has led to the current view that $m_\pi L > 6$ may in fact be needed to reliably determine g_A. However, we find that, as quantified by $m_\pi L$, the finite size effects are diminishing as m_π is lowered. This can be seen quite clearly in

[7] This is only true for the non-singlet moments, such as $\langle 1 \rangle_{\Delta u - \Delta d}$. The axial anomaly generates mixing for the singlet moments.

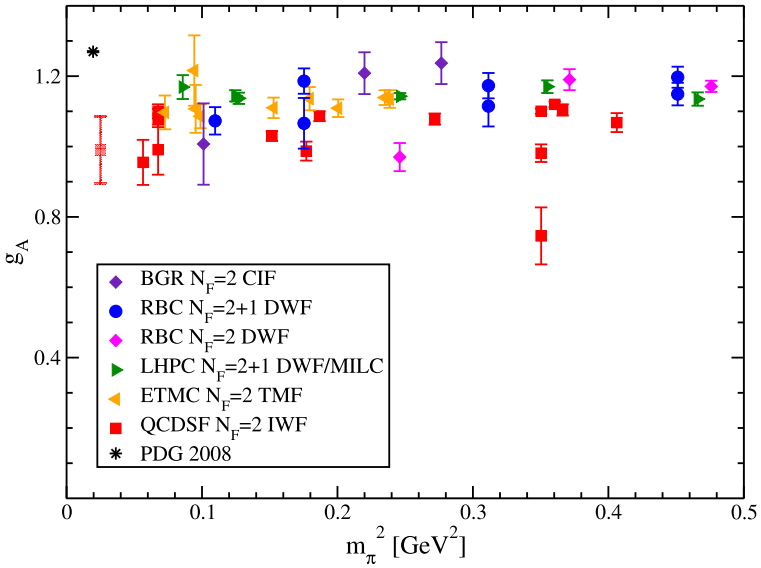

Figure 8: World's dynamical results for g_A. The lattice results are from [32, 33] (BGR), [25] (RBC $N_F = 2+1$), [19, 20] (RBC $N_F = 2$), [34] (LHPC), [35] (ETMC) and [24] (QCDSF). The experimental result is the PDG 2008 value [28]. The discrepancy between the lattice calculations and the experimental measurement and the scatter among the lattice calculations are both smaller than for $\langle x \rangle_{u-d}$ shown in Fig. 4.

Fig. 9 by examining the lighter pion mass calculations of both QCDSF and ETMC. It is possible that the volumes for these calculations at $m_\pi = 310$ MeV or 260 MeV may still be too small to see the asymptotic volume dependence. We can also consult chiral perturbation theory, which does allow for this sort of behavior; however, given that g_A is essentially flat for the largest volumes, one might reasonably question the use of chiral perturbation theory at these pion masses.

In order to attempt to estimate the infinite volume limits for the lattice calculations presented here, I simply require $m_\pi L > 6$. This may turn out to be an excessive requirement for low m_π, which would actually be good news regarding finite size effects, but it is clearly required for heavier pion masses. The lattice results satisfying this are shown in Fig. 10. As is clear from the figure, this restriction is very severe, however, the resulting lattice calculations show a strong level of agreement amongst themselves. The results are still lower than the experimental measurement, but, unlike for $\langle x \rangle_{u-d}$, only a mild curvature is required to reconcile the current calculations with the physical limit. In particular, notice that, with one exception, there is no systematic shift between the various collaborations. As mentioned earlier, the renormalization of g_A is generically easier than that of $\langle x \rangle_{u-d}$, and this lends a bit more support to the hypothesis that differences in renormalization may be driving part of the variation of $\langle x \rangle_{u-d}$ in Fig. 6. The one small exception is the result of QCDSF which is just slightly low compared to all the other calculations. However, this may be consistent with a small discrepancy in f_π, which renormalizes with the same factor as g_A, that is also present for QCDSF [36].

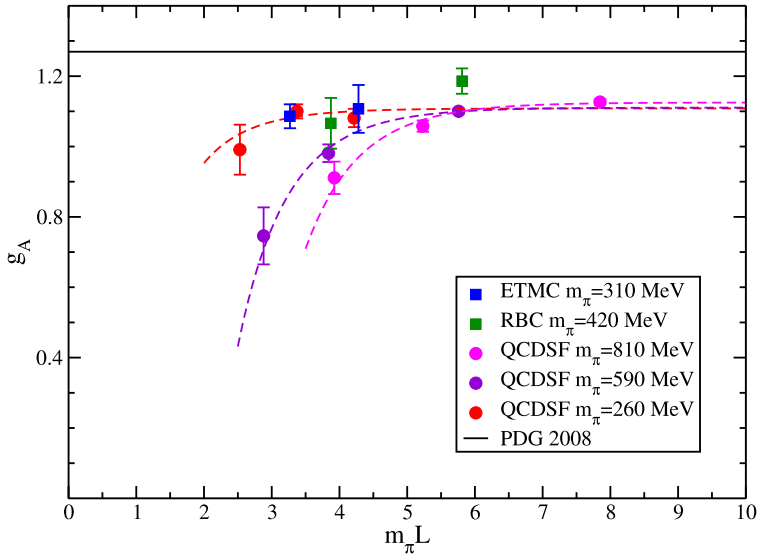

Figure 9: Finite size effects in g_A. The $m_\pi L$ dependence is shown for several calculations. The results at the heaviest pion masses indicate a significant finite size effect in g_A, suggesting that $m_\pi L$ of 6 may be necessary. But the light m_π results of QCDSF and ETMC may in fact be showing a weakening of the finite size effects in g_A as measured in terms of $m_\pi L$. The lattice results and experimental measurement are the same as in Fig. 8, and the curves are simple scaling fits to guide the eye.

4. Nucleon Charge

The charge of the nucleon, or any hadron, again appears to be an essentially trivial topic. There is no doubt that the proton has one unit of charge and that the neutron is, well, neutral. The certainty in our understanding of the nucleon's charge arises from the flavor symmetries of QCD, however, the distribution of this charge in the spatial degrees of freedom of the nucleon's constituents is not prescribed by symmetry and provides another probe of the dynamics of QCD within the nucleon. This idea leads to a broad range of calculations on the lattice and quickly involves the generalized parton distributions, but to avoid excessive complications and to explain the concepts in the simplest setting, I will discuss just the neutron charge [37].

4.1 Neutron Transverse Charge Distribution

Much of the interest in form factors originates with the interpretations that we can assign to them. There is now a rich field theoretic discussion dedicated to this issue, but in order to maintain our footing and retain a strong connection to the experimental measurements, it is valuable to remember that ultimately, the form factors parametrize the QCD contributions to cross sections, independent of any interpretation we attach to them.

$$\frac{d\sigma}{d\Omega} = \left(\frac{d\sigma}{d\Omega}\right)_{\text{Mott}} \left\{F_1^2 + \tau F_2^2 + 2\tau(F_1+F_2)^2 \tan^2(\theta/2)\right\}$$

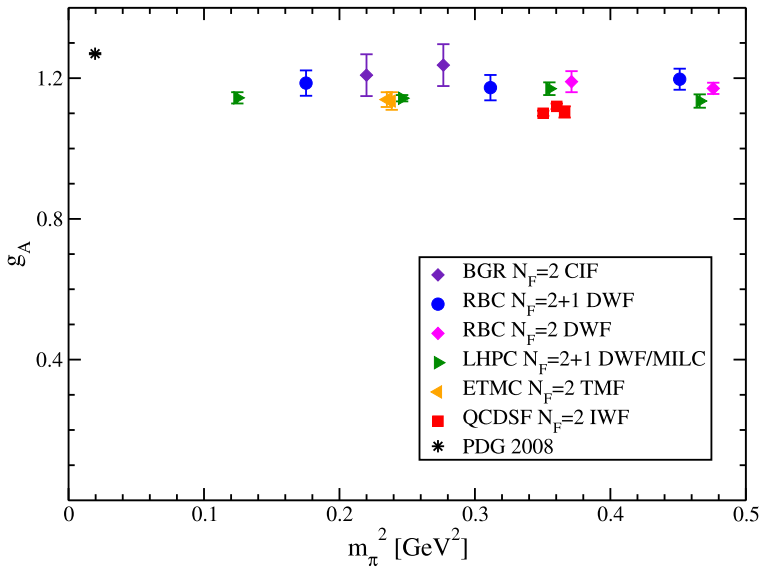

Figure 10: Results for g_A with $m_\pi L > 6$. The lattice results from Fig. 8 that satisfy $m_\pi L > 6$ are shown. All the lattice calculations, but one, are in statistical agreement. The results still underestimate the experimental value, but the discrepancy is much less severe than in $\langle x \rangle_{u-d}$. The QCDSF results are just slightly low. This may indicate some small systematic error in the renormalization or it may simply illustrate the lattice artifacts that are present in all the calculations.

Here $F_1(q^2)$ and $F_2(q^2)$ are the nucleon form factors and $\tau = q^2/(4m^2)$. For some in our community, this is where the discussion ends. That is, of course, a perfectly valid point of view. However, the understanding provided to us by the generalized parton distributions and the relationship to transverse quark distributions [38] allows us to go further.

Historically the form factors were interpreted as charge and magnetization densities. In particular the charge density was constructed from $G_E = F_1 - \tau F_2$ as

$$\rho_{3D}(\vec{r}) = \int \frac{d^3\vec{q}}{(2\pi)^3}\; e^{-i\vec{r}\cdot\vec{q}}\; \frac{m}{\sqrt{m^2+\vec{q}^2}} G_E(\vec{q}^2)\,.$$

This is plotted for the neutron in Fig. 11. There we see that the charge distribution is negative for large r. This is usually understood in terms of the pion cloud generated by $n \to p\pi^-$ fluctuations. Overall neutrality of the neutron forces the core to be positive leading to a negative charge radius.

But this picture is spoiled by relativistic corrections that enter as $(m\langle r\rangle)^{-1}$, where $\langle r\rangle$ is some relevant length scale for the charge distribution. These corrections would vanish in the non-relativistic limit $m \to \infty$ but are substantial for the nucleon. The introduction of the transverse distributions in the infinite-momentum frame (IMF) eliminates these corrections, which enter now as $(p_z\langle r\rangle)^{-1}$ with $p_z \to \infty$ defining the IMF. The transverse distributions [38] are given by

$$\rho_{2D}(\vec{b}) = \int \frac{d^2\vec{q}_\perp}{(2\pi)^2}\; e^{-i\vec{b}\cdot\vec{q}_\perp} F_1(\vec{q}_\perp^{\,2})\,.$$

This is shown for the neutron in Fig. 12. The distribution still has a negative tail for large r, but

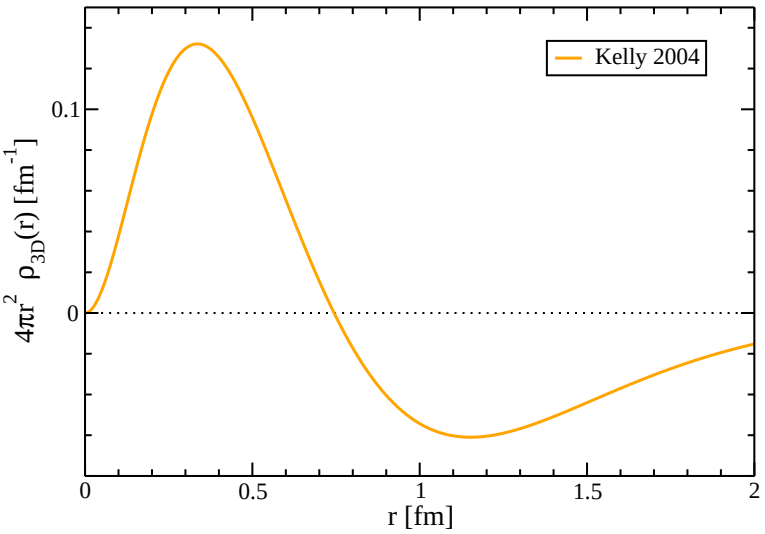

Figure 11: Naive 3d neutron charge distribution. The 3d Fourier transform of the G_E form factor gives the rest frame charge distribution of the nucleon up to relativistic corrections. The negative distribution at large r is interpreted as the pion cloud arising from the $n \to p\pi^-$ fluctuations. This gives rise to a negative charge radius for the neutron. The curves were generated by numerically integrating the Kelly 2004 parametrization of the nucleon form factors [39].

now we find a negative core. Furthermore, the charge radius is positive for the transverse charge distribution. Understanding this new view of the neutron is a challenge onto itself. Additionally, the introduction of the transverse coordinates in a field-theoretically clean manner opens many new avenues for investigation of hadron structure from lattice QCD.

4.2 Lattice Calculation of $\langle \mathbf{r^2} \rangle_{\mathbf{u-d}}$

As for the nucleon momentum and spin structure, I again introduce a benchmark observable that allows us to summarize the status of lattice calculations of form factors. Here I choose the isovector charge radius, $\langle r^2 \rangle_{u-d}$. As before, the flavor structure is $u-d$, so disconnected diagrams again vanish. Furthermore, this observable enters matrix elements of the vector current. These two facts combine to make $\langle r^2 \rangle_{u-d}$ an accurate quantity to calculate on the lattice. Additionally, all the lattice calculations can now use an exactly conserved vector current. This eliminates the need for any renormalization and simplifies the calculation significantly.

The form of the nucleon's electromagnetic interaction is given by

$$\langle p', s' | J^\mu | p, s \rangle = \overline{u}(p', s') \left\{ \gamma^\mu F_1(q^2) + i\sigma^{\mu\nu} \frac{q_\nu}{2m} F_2(q^2) \right\} u(p, s)$$

and the charge radius is then given by

$$\langle r^2 \rangle_{u-d} = -6 \left. \frac{dF_1^{u-d}}{dq^2} \right|_{q^2=0} .$$

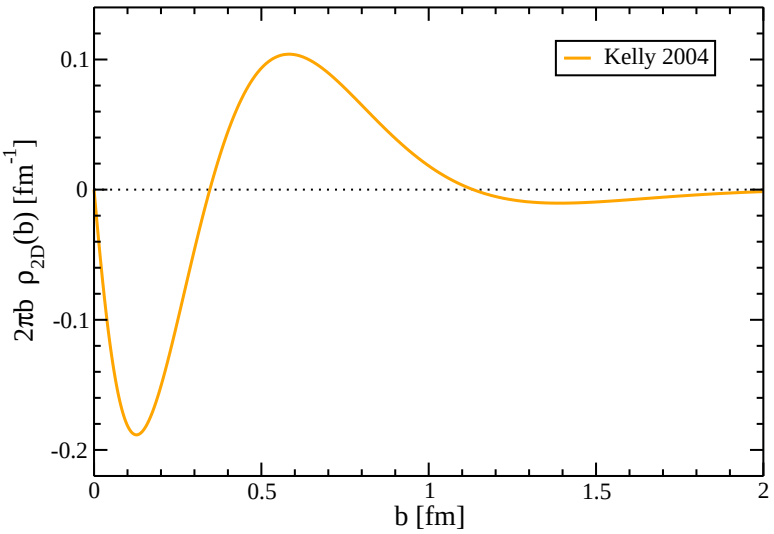

Figure 12: Transverse 2d neutron charge distribution. The 2d Fourier transform of the F_1 form factor results in the transverse charge distribution of the nucleon. Relativistic corrections are absent but the distribution must be understood in the infinite momentum frame. Notice the negative core, in contrast to Fig. 11. Also the charge radius is now positive in this frame. The distribution was constructed from the same form factor parametrization in Fig. 11.

The factor of 6 is the conventional choice, but a factor of 4 would instead give the correct transverse charge radius in the IMF. To avoid confusion, we stick to the conventional choice, but we should keep in mind the theoretically clean interpretation that is available for the transverse distribution.

In Fig. 13 I gather all the full QCD results for $\langle r^2\rangle_{u-d}$. It is immediately evident that all the lattice calculations show a remarkable agreement for this observable. The strong scatter that is present for $\langle x\rangle_{u-d}$ and to a lesser extent g_A is clearly absent for $\langle r^2\rangle_{u-d}$. This is particularly surprising given the fact that this quantity is expected to diverge in the chiral limit as indicated by the curve in Fig. 13. We might even expect large finite size effects in such a quantity. However, we must keep in mind that $\langle r^2\rangle_{u-d}$ is calculated from the slope of $F_1(q^2)$ at $q^2 = 0$ and that the momentum quantization imposed by a finite volume forces us to extract this slope using the first non-zero value of q^2, which satisfies $qL \approx 2\pi$. We may, in fact, be extrapolating from a region with weaker L dependence through the region with stronger L dependence. Ultimately, whatever the explanation, we find a near absence of volume dependence for $\langle r^2\rangle_{u-d}$.

Lacking any real guidance on the necessary volumes for $\langle r^2\rangle_{u-d}$, I simply follow the conventional wisdom and take $m_\pi L > 4$. These lattice results are shown in Fig. 14. An optimist may find a mild increase, but this would be hard to defend strongly. Additionally, this observable requires much more than a mild increase to agree with the experimental value at the physical point. But it does appear that all the calculations seem to agree. Given that $\langle r^2\rangle_{u-d}$ requires no renormalization, this is consistent with the speculation suggesting that renormalization may be partially culpable for

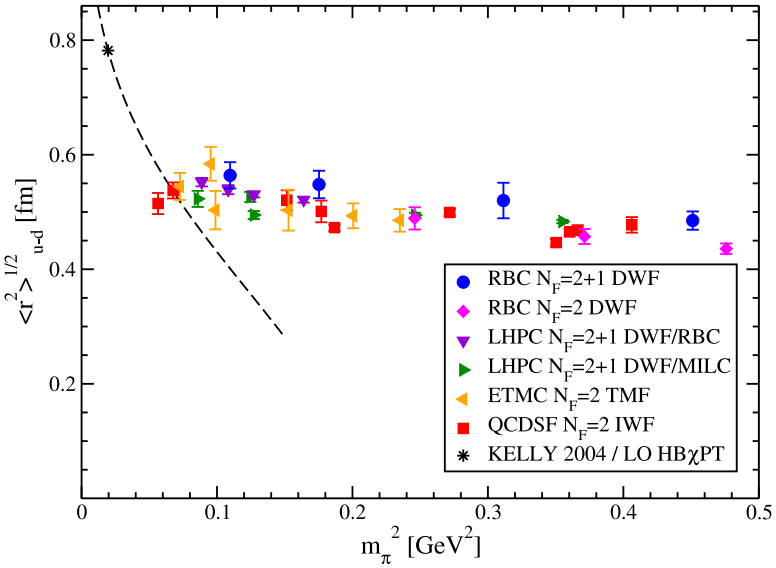

Figure 13: World's dynamical results for $\langle r^2 \rangle_{u-d}^{1/2}$. The lattice calculations are [25] (RBC $N_F = 2+1$), [19, 20] (RBC $N_F = 2$), [40] (LHPC/MILC), [41] (LHPC/RBC), [35] (ETMC) and [24] (QCDSF). The experimental result comes from the Kelly 2004 parametrization of the form factors [39]. The leading order heavy baryon chiral perturbation theory prediction (LO HBχPT) contains no unknown low energy constants other than $\langle r^2 \rangle_{u-d}^{1/2}$ and is logarithmically divergent as $m_\pi \to 0$. One might, therefore, expect substantial finite size effects in this quantity, but this does not appear to be the case.

the systematic variation in $\langle x \rangle_{u-d}$ discussed earlier. Despite the fact that this observable still shows a significant discrepancy with the experimental result, the agreement amongst all the lattice groups is encouraging.

5. Conclusions and Outlook

In order to illustrate the status and promise of lattice calculations of hadron structure, I chose to review three benchmark observables that represent the broad range of hadronic physics that we can address on the lattice: the momentum fraction, axial charge and charge radius of the nucleon. Nearly all the lattice groups have pushed the pion mass towards 300 MeV or lower and some are now breaking through 200 MeV. This is an enormous accomplishment, but unfortunately most hadronic observables are failing to show the long-sought chiral curvature. Independent of the expectations of chiral perturbation theory, the three benchmark observables still do not show a convincing approach to the experimental results.

The obvious conclusion is that yet lighter, and maybe even physical, pion masses will be required. This may be the case, but we should not do this at the expense of other systematic errors. Finite size effects must remain a concern as we lower m_π. Both $\langle x \rangle_{u-d}$ and g_A demonstrate that the volume dependence can have a non-trivial dependence on m_π and our conventional rule-of-thumb that $m_\pi L \approx 4$ may not necessarily be sufficient for all quantities.

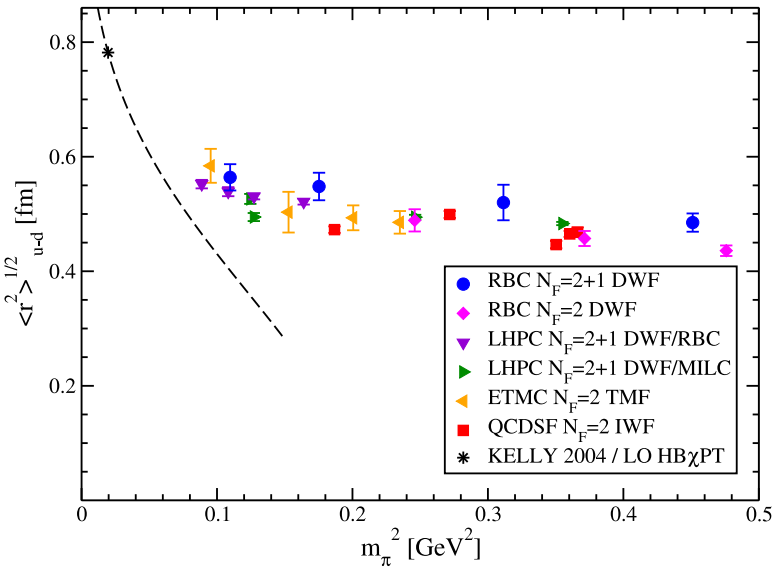

Figure 14: Large volume results for $\langle r^2 \rangle^{1/2}_{u-d}$. Due to momentum quantization at finite volume, one can not easily calculate the form factors at the low Q^2 needed to determine $\langle r^2 \rangle^{1/2}_{u-d}$ while also working at small volume. Lacking any detailed knowledge of the finite size effects in $\langle r^2 \rangle^{1/2}_{u-d}$, only the results from Fig. 13 with $m_\pi L > 4$ are shown. There is general agreement among all the lattice groups and a mild increase as m_π is lowered. However $\langle r^2 \rangle^{1/2}_{u-d}$ is not yet rising nearly as fast as it needs to match onto the experimental measurement.

Lattice artifacts are still a concern, if only because so few groups have seriously examined them. The agreement of the groups for $\langle r^2 \rangle_{u-d}$ might indicate weak artifacts for some quantities, but the systematic shifts between the groups for $\langle x \rangle_{u-d}$ is a warning that renormalization, an essential part of the continuum limit for most quantities of interest, may be partially responsible for these problems. The role of renormalization is further implicated by the general agreement of the groups for the renormalization free ratio of $\langle x \rangle_{u-d} / \langle x \rangle^{\text{ref}}_{u-d}$. In fact, the progression from $\langle x \rangle_{u-d}$ (requiring a scale-dependent renormalization) to g_A (requiring only a finite renormalization) to $\langle r^2 \rangle_{u-d}$ (requiring no renormalization) will be a strong test of our control of renormalization issues.

These systematic effects will be a part of any critical review of lattice calculations, but we should remember the rich QCD physics that provides the motivation for these calculations. Each of the benchmark observables is a stand-in for a broad range of experimentally relevant and intellectually interesting observables: the decomposition of momentum among the nucleon's constituents, the nature of the nucleon's spin and the distribution of the nucleon's charge. Apart from these observables, Lattice 2009 saw a sizeable effort to study strangeness in the nucleon, results for the pion, delta and other hadrons, and a range of exploratory calculations. Clean control of systematics and a continued push toward the physical pion mass will ultimately allow detailed calculations that will complement the experimental programs and advance our insight into hadron structure.

Acknowledgments

I gratefully appreciate the many conversations and email exchanges with colleagues while preparing for the Lattice 2009 conference. I would like to thank D. Alexandrou, G. Bali, W. Bietenholz, T. Blum, T. Doi, M. Engelhardt, W. Freeman, Ph. Hägler, P.-A. Harraud, T. Hemmert, K. Jansen, T. Kaneko, T. Korzec, M. Lin, Z. Liu, D. Mohler, B. Musch, J. Negele, H. Ohki, S. Ohta, J. Osborn, G. Schierholz, W. Schroers, T. Streuer, K. Takeda, N. Ukita, A. Walker-Loud and J. Zanotti. Additionally, this work was supported by the DFG Sonderforschungsbereich/Transregio SFB/TR9-03

References

[1] J. M. Zanotti. Investigations of hadron structure on the lattice. *arXiv:0812.3845*, 2008.

[2] Ph. Hägler. Progress in hadron structure physics on the lattice. *PoS*, LAT2007:013, 2007.

[3] K. Orginos. Recent lattice QCD results on nucleon structure. *PoS*, LAT2006:018, 2006.

[4] Ph. Hägler. Hadron structure from lattice quantum chromodynamics. *arXiv:0912.5483*, 2009.

[5] R. D. Young and A. W. Thomas. Recent results on nucleon sigma terms in lattice QCD. *arXiv:0911.1757*, 2009.

[6] M. R. Whalley, D. Bourilkov, and R. C. Group. The Les Houches Accord PDFs (LHAPDF) and LHAGLUE. *arXiv:hep-ph/0508110*, 2005.

[7] A. D. Martin, W. J. Stirling, R. S. Thorne, and G. Watt. Parton distributions for the LHC. *Eur. Phys. J.*, C63:189–285, 2009.

[8] R. Brock et al. Handbook of perturbative QCD: Version 1.0. *Rev. Mod. Phys.*, 67:157–248, 1995.

[9] P. M. Nadolsky et al. Implications of CTEQ global analysis for collider observables. *Phys. Rev.*, D78:013004, 2008.

[10] S. Alekhin, J. Blumlein, S. Klein, and S. Moch. The 3-, 4-, and 5-flavor NNLO Parton from Deep-Inelastic-Scattering Data and at Hadron Colliders. *arXiv:0908.2766*, 2009.

[11] J. Blumlein, H. Bottcher, and A. Guffanti. Non-singlet QCD analysis of deep inelastic world data at $O(\alpha_s^3)$. *Nucl. Phys.*, B774:182–207, 2007.

[12] J. Blumlein, H. Bottcher, and A. Guffanti. Non-singlet QCD analysis of the structure function F_2 in 3-loops. *Nucl. Phys. Proc. Suppl.*, 135:152–155, 2004.

[13] P. Jimenez-Delgado and E. Reya. Dynamical NNLO parton distributions. *Phys. Rev.*, D79:074023, 2009.

[14] A. D. Martin, W. J. Stirling, R. S. Thorne, and G. Watt. Uncertainties on α_s in global PDF analyses and implications for predicted hadronic cross sections. *Eur. Phys. J.*, C64:653–680, 2009.

[15] S. Alekhin, K. Melnikov, and F. Petriello. Fixed target Drell-Yan data and NNLO QCD fits of parton distribution functions. *Phys. Rev.*, D74:054033, 2006.

[16] C. Allton et al. 2+1 flavor domain wall QCD on a (2 fm)^3 lattice: light meson spectroscopy with $L_s = 16$. *Phys. Rev.*, D76:014504, 2007.

[17] C. Allton et al. Physical Results from 2+1 Flavor Domain Wall QCD and SU(2) Chiral Perturbation Theory. *Phys. Rev.*, D78:114509, 2008.

[18] S. Ohta. Private Communication for RBC.

[19] H.-W. Lin, T. Blum, S. Ohta, S. Sasaki, and T. Yamazaki. Nucleon structure with two flavors of dynamical domain- wall fermions. *Phys. Rev.*, D78:014505, 2008.

[20] Y. Aoki et al. Lattice QCD with two dynamical flavors of domain wall fermions. *Phys. Rev.*, D72:114505, 2005.

[21] Ph. Hägler et al. Nucleon Generalized Parton Distributions from Full Lattice QCD. *Phys. Rev.*, D77:094502, 2008.

[22] P.-A. Harraud. Private Communication for ETMC.

[23] Z. Liu. Private Communication for ETMC.

[24] J. Zanotti. Private Communication for QCDSF.

[25] T. Yamazaki et al. Nucleon form factors with 2+1 flavor dynamical domain-wall fermions. *Phys. Rev.*, D79:114505, 2009.

[26] X.-D. Ji. Off-forward parton distributions. *J. Phys.*, G24:1181–1205, 1998.

[27] H. Abele. The neutron. Its properties and basic interactions. *Prog. Part. Nucl. Phys.*, 60:1–81, 2008.

[28] C. Amsler et al. Review of particle physics. *Phys. Lett.*, B667:1, 2008.

[29] A. Airapetian et al. Precise determination of the spin structure function g_1 of the proton, deuteron and neutron. *Phys. Rev.*, D75:012007, 2007.

[30] I. Balitsky and X.-D. Ji. How much of the nucleon spin is carried by glue? *Phys. Rev. Lett.*, 79:1225–1228, 1997.

[31] V. Barone, T. Calarco, and A. Drago. Gluon spin in a quark model. *Phys. Lett.*, B431:405–409, 1998.

[32] C. Gattringer et al. Hadron Spectroscopy with Dynamical Chirally Improved Fermions. *Phys. Rev.*, D79:054501, 2009.

[33] D. Mohler. Private Communication for BGR.

[34] J. Negele. Private Communication for LHPC.

[35] T. Korzec. Private Communication for ETMC.

[36] K. Jansen. Lattice QCD: a critical status report. *PoS*, LATTICE2008:010, 2008.

[37] G. A. Miller. Charge Density of the Neutron. *Phys. Rev. Lett.*, 99:112001, 2007.

[38] M. Burkardt. Impact parameter dependent parton distributions and off-forward parton distributions for $\zeta \to 0$. *Phys. Rev.*, D62:071503, 2000.

[39] J. J. Kelly. Simple parametrization of nucleon form factors. *Phys. Rev.*, C70:068202, 2004.

[40] J. D. Bratt et al. Nucleon structure from mixed action calculations using 2+1 flavors of asqtad sea and domain wall valence fermions. *arXiv:1001.3620*, 2010.

[41] S. N. Syritsyn et al. Nucleon Electromagnetic Form Factors from Lattice QCD using 2+1 Flavor Domain Wall Fermions on Fine Lattices and Chiral Perturbation Theory. *arXiv:0907.4194*, 2009.